

Annals of the American Association of Geographers



ISSN: (Print) (Online) Journal homepage: https://www.tandfonline.com/loi/raag21

Coupled Adaptive Cycles of Shoreline Change and Households in Deltaic Bangladesh: Analysis of a 30-Year Shoreline Change Record and Recent Population Impacts

Thomas W. Crawford , Munshi Khaledur Rahman , Md. Giashuddin Miah , Md. Rafiqul Islam , Bimal Kanti Paul , Scott Curtis & Md. Sariful Islam

To cite this article: Thomas W. Crawford, Munshi Khaledur Rahman, Md. Giashuddin Miah, Md. Rafiqul Islam, Bimal Kanti Paul, Scott Curtis & Md. Sariful Islam (2020): Coupled Adaptive Cycles of Shoreline Change and Households in Deltaic Bangladesh: Analysis of a 30-Year Shoreline Change Record and Recent Population Impacts, Annals of the American Association of Geographers, DOI: 10.1080/24694452.2020.1799746

To link to this article: https://doi.org/10.1080/24694452.2020.1799746

	Published online: 23 Sep 2020.
	Submit your article to this journal $oldsymbol{arGamma}$
Q ^L	View related articles $oxize{\mathbb{Z}}$
CrossMark	View Crossmark data 🗗



Coupled Adaptive Cycles of Shoreline Change and Households in Deltaic Bangladesh: Analysis of a 30-Year Shoreline Change Record and Recent Population Impacts

Thomas W. Crawford, * Munshi Khaledur Rahman, † Md. Giashuddin Miah, † Md. Rafiqul Islam, * Bimal Kanti Paul, * Scott Curtis, * and Md. Sariful Islam*

*Department of Geography, Virginia Tech

†Department of Geology and Geography, Georgia Southern University

‡Vice Chancellor, Bangabandhu Sheikh Mujibur Rahman Agricultural University

#Department of Agronomy, Bangabandhu Sheikh Mujibur Rahman Agricultural University

§Department of Geography and Geospatial Sciences, Kansas State University

¶Department of Geography, Planning and Environment, East Carolina University

This research investigates the spatiotemporal dynamics of shoreline change and associated population impacts in deltaic Bangladesh. This region is among the world's most dynamic deltas due to monsoon precipitation that drives tremendous discharge and sediment volumes from the Ganges-Brahmaputra-Meghna drainage basin. Theoretically, it draws on the concept of adaptive cycles that theorizes systems transitioning through phases of growth, conservation, release (collapse), and reorganization, with a focus on the cycle's release (collapse) phase and coupled linkages between the natural system of shoreline change and social system of household behavior. We use Landsat imagery to produce and describe a thirty-year record of shoreline change for an 80-km stretch of the Lower Meghna estuary. Household survey data characterized population impacts and risk perception for a subregion with high erosion rates. Results identified significant space-time differences and patterns of shoreline change and population impacts consistent with the adaptive cycle. North, central, and south regions exhibited statistically significant differences in space-time patterns of shoreline change. Substantial numbers of households reported displacement due to riverbank erosion and high levels of experience and worry about future displacement. Results demonstrate how geospatial analysis of a multidecade record of shoreline change along with analysis of household survey data can identify regions most vulnerable to riverbank erosion with implications to inform mitigation and adaptation. This work adds empirical demonstration of coupled adaptive cycles to the literature. Limitations and complexities of the adaptive cycle framework are discussed. Key Words: adaptive cycle, erosion/accretion, household survey, remote sensing, spatiotemporal analysis.

Settlements in coastal lowlands are vulnerable to risks associated with environmental processes such as coastal erosion, sea-level rise (SLR), higher intensity storm events, and altered rainfall regimes that create the potential for increased risk contributing to potential social and economic disruption. Many coastal lowlands in developing countries, particularly delta environments, are heavily populated with among the highest densities in the world, with predicted future population growth (Small et al. 2018). These economically marginalized populations are likely to be disproportionately affected (McGranahan, Balk, and Anderson 2007). Magnitudes and severities

of affected populations have the potential to threaten economic and political stabilities of host countries (Smith 2007; Ackerman 2008; Jasparro and Taylor 2008).

This research investigates the spatiotemporal dynamics of shoreline change and associated population impacts in deltaic Bangladesh. Theoretically, it draws on the concept of adaptive cycles (Holling 1986; Gunderson and Holling 2002) that theorizes systems transitioning through phases of growth, conservation, release (collapse), and reorganization. This study's focal system of the Lower Meghna estuary is a coupled human—natural system in which

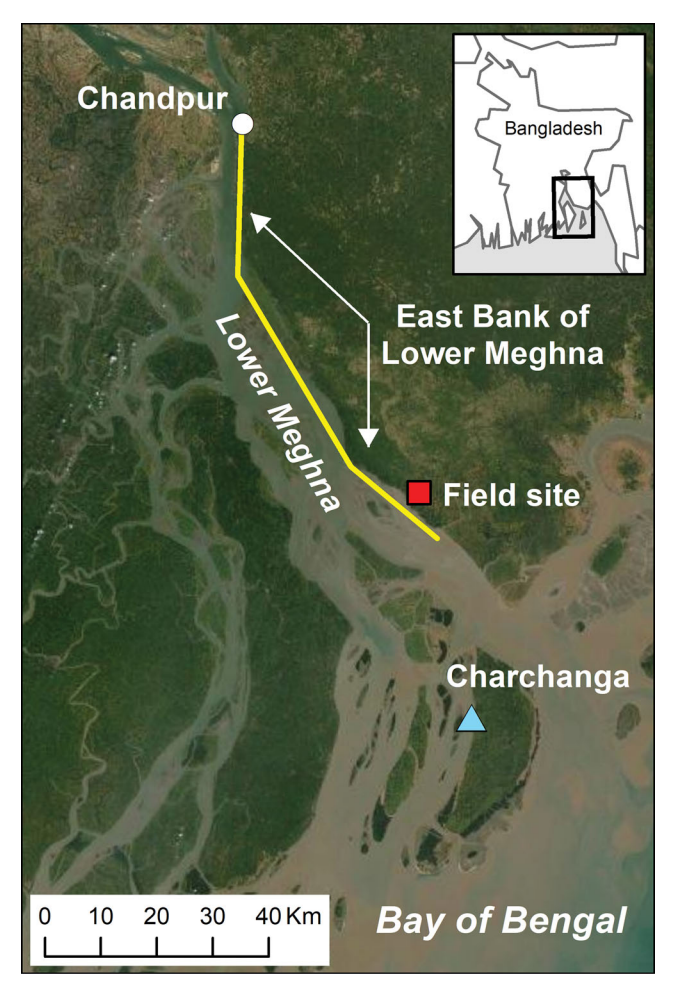


Figure 1. Study shoreline—east bank of the Lower Meghna estuary. The red square indicates the location of household survey field site in Lakshmipur district; the white circle indicates the northern terminus at Chandpur (city); and the blue triangle is the Charchanga tidal station.

the population relies on ecosystem services and functions of the delta for livelihood strategies. The delta functions according to natural functions of delta system dynamics influencing biophysical patterns and processes. We present a coupling of both household adaptive cycles (social system) and landform adaptive cycles (natural system) focusing on the adaptive cycle's release (collapse) phase described in more detail later.

The Ganges-Brahmaputra-Meghna (GBM) delta is an Asian megadelta. Asian megadeltas are large deltas associated with major Asian river systems (Chen and Saito 2011). Asian megadeltas include the Indus, GBM, Irrawaddy, Mekong, Red, Pearl, Changjiang (Yangtze), and Huanghe (Yellow; Woodroffe 2010). They are particularly noteworthy due to their high population concentrations, the

large size of their contributing upstream basins, the location of source headwaters in the Himalaya massif, and the importance of monsoon dynamics for rainfall delivery and river discharge dynamics. Situated at outlet points through which basin discharge flows, Asian megadeltas are profoundly influenced by processes occurring at basin-wide and regional scales. The GBM delta is the largest of the Asian megadeltas, covering an extent of more than 100,000 km² (Woodroffe et al. 2006). It is among the world's most dynamic deltas due to annual monsoonal rainfall that drives tremendous discharge volumes influencing sediment transport dynamics and associated erosion and accretion landform processes (Chowdhury and Ward 2004; Mikhailov and Dotsenko 2007; Woodroffe and Saito 2011; Wilson and Goodbred 2015).

This study analyzes coastal shoreline change and its impacts on human population for an area located at the main terminus of the GBM delta (Figure 1). Within this major, multiriver system, rivers combine to form the Lower Meghna River and estuary with hydrodynamics that are largely fluvial dominated (Woodroffe and Saito 2011) along a gradient that becomes more tidally influenced with increased proximity to the Bay of Bengal.

Adaptive Cycles: Linkage of Natural and Social Systems

Both natural and human dimensions of riverbank erosion in the Lower Meghna system are particularly salient due to the severe magnitude of erosion coupled with the large population in this delta region. Our work links riverbank erosion with impacts and responses of the social system. Theoretically, we draw from the concept of adaptive cycles linking adaptive cycles of aspects of the natural system to the social system. Although this work is specific to the Lower Meghna system, our theoretical understanding of this system's coupled adaptive cycles has potential translation to other coupled systems where disturbance processes of natural and social systems are linked.

As originally theorized by Holling (1986), within an adaptive cycle (Figure 2) a system might be located in phases of growth (r), conservation (K), release (Ω), and reorganization (α). The growth stage is an entrepreneurial, pioneering stage where exploitation and sequestering of resources occur.

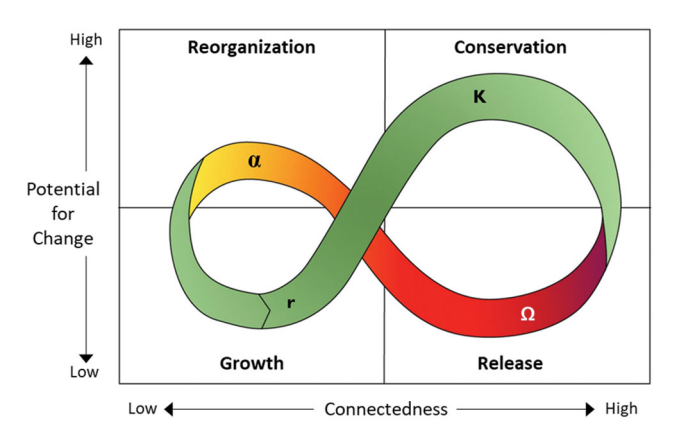


Figure 2. Adaptive cycle (after Gunderson and Holling 2002).

This is followed by a conservation stage characterized by organizational consolidation and accumulation. This can be thought of as a mature stage, but also as a stage where natural or social systems might be poised for collapse should a disturbance event occur. On collapse, a release stage unleashes organization and energy accumulated during the conservation stage. The reorganization phase is a period of restructuring, renewal, and reassembly of system components. The adaptive cycle was originally developed and applied to natural ecological systems and has been extended to investigation of social systems and coupled human-natural systems (see Rasmussen and Reenberg 2012; Goulden et al. 2013; Holdschlag and Ratter 2013). Holling's adaptive cycle is closely related to the concept of panarchy, which posits a nested set (nested by time-space scales) of hierarchically organized adaptive cycles (Gunderson and Holling 2002) that interact via cross-scale interactions and linkages. Much of the adaptive cycle literature employs this broader panarchy concept along with resilience. Our work anticipates a similar approach; here, though, we focus more modestly on articulating and demonstrating the presence of linked adaptive cycles interacting across natural and human systems for the Lower Meghna system without specifying hierarchically scaled relationships.

Figure 2 and Table 1 depict and describe an adaptive cycle framework that describes linked adaptive cycles for riverbank erosion and household dynamics in the Lower Meghna system littoral. This lower delta plain region contains floodplain sedimentary landforms known as char or charlands, on which deposition from the GBM basin has built landforms supporting significant populations engaged in household livelihood activities including farming, fishing,

and mixed employment strategies (Wilde 2000; Sarker et al. 2003; Wilde 2011). The natural processes of the Lower Meghna system in the Bangladesh delta (Allison 1998a, 1998b; Kuehl et al. 2005; Wilson and Goodbred 2015) involve regular episodes of landform erosion and accretion that conceptually transition through the various phases of the adaptive cycle with phases of growth, conservation, release, and reorganization. The system builds land via sediment deposition, which matures and stabilizes, and the system destroys land via erosion. This process repeats over time. These natural system processes are linked to household livelihood processes due to the social disturbance caused by riverbank erosion, which severely affect households that become displaced and enter the Ω -release (collapse) phase due to lost land resources and associated livelihood resources. Households affected by riverbank erosion are challenged to negotiate and transition through the adaptive cycle involving α-reorganization and r-growth (reestablishment) and succeeding K-conservation (restabilization and maturation) phases. Using the adaptive cycle framework, we seek to describe and understand patterns of riverbank erosion as a disturbance event of the Ω -release (collapse) phase and how it relates to adaptive cycles of households within the social system. We do so by presenting quantitative geospatial analysis of a thirty-year record on shoreline change of an 80-km stretch of the eastern bank of the Lower Meghna estuary. We also present analysis of household survey data (n = 407) that measures household experience and perception of erosion. The survey was conducted for households along a 15-km shoreline reach in Lakshmipur district located in the far southern portion of the fuller 80-km coastline reach (Figure 1).

Shoreline Change: Riverbank Erosion

Riverbank erosion is a recurring problem in Bangladesh that annually causes tens of thousands of people to become homeless (Figure 3). Bangladesh's Centre for Environmental and Geographic Information Services predicted that in 2014 more than 36,000 people would be displaced due to erosion along the banks of Bangladesh rivers. The Centre for Environmental and Geographic InformationServices estimated net erosion of 162,000 hectares between 1973 and 2018 along banks of major Bangladesh rivers and tributaries (Ullah, Islam, and Alam 2019).

Table 1. Description of the four phases of adaptive cycles of littoral landforms (char lands) and households located in the Lower Meghna estuary, Bangladesh

Phase	Description	Potential for change	Connectedness
Littoral landforms r-Growth			
	 Incremental sediment accumulation and accretion Growth trajectory: subtidal—intertidal—supratidal 	Declines as growth trajectory progresses	Low but starts to increase with landform emergence/ connection to mainland
K-Conservation	meeridai–supratidai		
	Land has emerged and stabilizesVegetation establishment	 Becomes high and poised for collapse 	 Increases as new landform becomes connected to mainland
Ω -Release			
	 Site-specific collapse of landform due to riverbank erosion Loss of land, soil, vegetation 	 Suddenly declines pending potential reorganization 	 High, but connection to mainland is suddenly broken
α-Reorganization			
	 Sites in fluvial/estuarine nonland state influenced by hydrological discharge and sediment dynamics Potential to enter growth phase of land reestablishment 	Relatively high for future landform reestablishment	Low due to broken connection with mainland
Households			
r-Growth	 Household formation, land acquisition, homestead establishment Engagement in economic activities and 	Declines as household establishment progresses	• Low initially due to flux state but starts to increase as household regains footing and livelihood activities
K-Conservation	experimentation		
	 Household progresses/ progressed through demographic life cycle; social networks formed Established household livelihood activities 	 Becomes high pending likely future crisis related to riverbank erosion 	 Increases as household has emerged from crisis and is reintegrated to livelihood activities
Ω -Release			
	 Land and homestead lost to erosion; severe negative impacts on household livelihood Household displacement and crisis 	Suddenly declines pending potential reorganization	 High at crisis onset but crisis transitions household to an in-flux state where prior livelihood connections are broken

(Continued)

Table 1. (Continued).

Phase	Description	Potential for change	Connectedness
α-Reorganization			
	 Household in state of flux and seeking reestablishment Migration to new site and potential to enter growth phase of household reestablishment 	Relatively high for future household reestablishment	Low due to in-flux state as household seeks to reestablish livelihood connections



Figure 3. Shoreline change due to riverbank erosion, Ramgati Upazila, Bangladesh, January 2018.

Coastal Bangladesh is commonly regarded as being highly vulnerable to SLR; however, addressing SLR impacts on erosion and accretion and net land loss and gain is complicated by the complex diversity of the region's coastal physical geography (Brammer 2014). Given the 1988 to 2018 timescale of this research, SLR likely has had negligible impacts on shoreline change for our study region; however, Brammer (2014) stated future longer term potential adverse impacts of SLR, including inland advance of the saltwater front in western parts of the Ganges tidal floodplain, impedance of drainage for areas east

of the Lower Meghna river, and increased erosion rates of older char islands in the Meghna estuary.

A substantial literature has quantified riverbank erosion patterns for noncoastal, interior regions of Bangladesh (e.g., Jamuna and Padma Rivers) using remotely sensed imagery (Khan and Islam 2003; Baki and Gan 2012). Other research has analyzed erosion for the exterior coastal region facing the Bay of Bengal (Rahman, Dragoni, and El-Masri 2011; Sarwar and Woodroffe 2013), as opposed to our interior estuarine coast of the Lower Meghna estuary. Much of the shoreline change research and

Table 2. Selected erosion rates from delta and coastal research

Citation	Region	Temporal resolution	Spatial resolution	Erosion rates
Bangladesh coast				
Sarwar and Woodroffe (2013)	Bangladesh	10 years	30 m	-35 to -285 m/year
Islam et al. (2016)	Bangladesh	4 years	30, 60 m	0 to −100 m/year
Salauddin et al. (2018)	Bangladesh	5 years	30 m	-3 to -130 m/year
Other delta regions				
Dada et al. (2016)	Niger River delta	5, 10 years	30 m	-4 to -30 m/year
Ghoneim et al. (2015)	Nile River delta	2 years	1.84, 57 m	-30 m/year
Esmail, Mahmod, and Fath (2019)	Nile River delta	10 years	15, 30 m	-5 to -70 m/year
Zhang et al. (2018)	Yellow River delta	20 years	30, 60 m	-25 to -35 m/year
Qiao et al. (2018)	Yangtze River delta	5 years	1.8, 30 m	-30 m/year
Indian coast				
Jana et al. (2014)	India coast	10 years	30, 60 m	-1 to -10 m/year
Natesan et al. (2015)	India coast	10 years	30, 60 m	-7 to -40 m/year
Rani et al. (2018)	India coast	10 years	30 m	-2 to -80 m/year
Baral et al. (2018)	India coast	3 years	23.5, 60 m	-1 to -10 m/year
Jayanthi et al. (2018)	India coast	10 years	30, 60 m	0 to -55 m/year

Note: Temporal resolution is temporal grain (interval). Several studies spanned multiple decades of extent. Erosion rates were rounded to show generalized information on relative magnitudes.

elsewhere uses Landsat imagery and geospatial analysis to quantify rates of shoreline change.

Table 2 summarizes selected representative research of shoreline change in Bangladesh, other delta regions, and coastal India. These studies reveal that coastal Bangladesh has the highest erosion rates at greater than 100 m per year, compared to other reported regions. Compared to Bangladesh's interior rivers, relatively little research has investigated erosion in the Lower Meghna estuary (Paul and Rashid 2017; but see Hussain et al. 2014; Ahmed et al. 2018).

Objectives

This research aims to improve understandings of shoreline change for a defined study area of the Lower Meghna estuary (Figure 1). Specific objectives include the following:

- 1. Produce shorelines spanning a thirty-year period from classified Landsat imagery for the years 1988, 1998, 2008, and 2018.
- 2. Characterize the space-time variability of shoreline change at decadal and thirty-year temporal scales.
- 3. Quantify household experience, perception, and risk of riverbank erosion for a sample of households located along a 15-km shoreline reach.

These objectives are important for multiple reasons. First, addressing these objectives within the theoretical framework of coupled adaptive cycles is an

important contribution that empirically addresses the adaptive cycle concept, which has typically been addressed by heuristic or metaphorical treatment (Sundstrom and Allen 2019), although empirical research of adaptive cycles is increasing as described earlier.

Second, there is a need to rigorously analyze shoreline change for the Lower Meghna estuary, which has received much less attention compared to the exterior coast and the interior rivers in Bangladesh. Recent news reports highlight the extreme severity of erosion hazards in this region (Correspondent 2019). Further justification comes from preliminary work using WorldPop 100 m resolution gridded population data (Stevens et al. 2015), enabling us to estimate that in 2010 approximately 720,000 people lived within 5 km of our study's 80km shoreline, indicating a large and potentially vulnerable population. To preview results, erosion rates in this densely populated region are among the highest rates in the world and in some cases at extreme levels.

Our work also anticipates the need for long-term multidecadal analysis at finer temporal scales. The presence of decadal-scale variation we present here will suggest variation occurring at an even finer annual scale (or finer) erosion and accretion dynamics. This is important for our study area and others because affected populations and policy leaders often must undertake adaptive or mitigative behaviors at timescales finer than decadal scales.

Tidal level (mm)^a Image date Representative dry season year Landsat platform and resolution 2/19/1988 1988 3,120 Landsat 5 TM (30 m) 1998 2,640 Landsat 5 TM (30 m) 2/14/1998 1,300^a 12/16/2007^b 2008 Landsat 7 TM (30 m) 1/4/2018 2018 Unknown^c Landsat 8 OLI (30 m)

Table 3. Landsat images from Path 137, Row 44 used in analyses

Notes: "Tidal levels are observed and estimated levels at Charchanga station. The 1,300 mm level for 12/16/2007 is estimated via regression relationship as described in text.

Data and Methods

Landsat Images and Tidal Data

Landsat images were selected (Table 3) based on inspection of imagery available from the U.S. Geological Survey Global Visualization View Web site (USGS 2018). All images had a 30-m pixel resolution. Criteria guiding image selection were as follows:

- 1. Full shoreline coverage of approximately 80 km of shoreline from Chandpur (north) to a southern terminus in Lakshmipur district (Figure 1).
- 2. Approximate January–February dry season anniversary dates with cloud-free coverage.
- 3. Similar and preferably high tidal levels at the Charchanga tidal station (Figure 1) occurring at 10:00 a.m. local time corresponding to the approximate time of scene acquisition.

Landsat path/row 137 (path) and 44 (row) provides full coverage of the 80-km shoreline. January and February dry season dates were preferred for two reasons. First, the monsoon climate causes many images acquired outside of the dry season to be cloud covered. Second, the majority of erosion occurs during the monsoon period associated with higher precipitation-related river discharge. Shorelines derived during successive dry seasons therefore effectively capture before and after snapshots of the shorelines, revealing the effects of the dominant monsoon period of erosion.

Tidal level is an important consideration for shoreline mapping. Ideally, levels synchronized to image acquisition dates and times would be identical and as high as possible to represent the high-water line. Tidal-level data are not consistently available at multiple locations spanning the shoreline for 1988 to 2018. We used tidal data (Table 3) from two stations: Charchanga and Chandpur (Figure 1). Hourly

Charchanga data were available for 1998 to 2000 from the Permanent Service for Mean Sea Level (n.d.) based in Liverpool, UK, although the original source was the Bangladesh Water Development Board (n.d.). Three-hour Chandpur data covering 1995 to 2018 were acquired directly from the Bangladesh Water Development Board. Source data were reported in millimeter units.

Tidal levels for Charchanga after 2000 and at 10:00 a.m. local time were estimated via linear regression using the Chandpur 9:00 a.m. water level as a predictor. Data were limited to December through February for the years 1995 to 2000 where tidal-level data existed for both Charchanga and Chandpur. Regression results (n = 445, $R^2 = 0.96$) were used to estimate Charchanga levels at 10:00 a.m. for 1995 through 2000, closely corresponding to the approximate image acquisition times. Applying regression results to predict 2001 through 2018 Charchanga tidal levels, we are able to confidently state water levels for the Charchanga tidal station for all but the 2018 image date. A 2018 estimate was not possible because corresponding 2018 data for Chandpur were not available.

Landsat platforms included Landsat-5 Thematic Mapper (TM), Landsat-7 Enhanced Thematic Mapper (ETM), and Landsat-8 Operational Land Imager (OLI; Table 3). We focused on the eastern shoreline of the Lower Meghna shoreline because of related social science field work we are conducting in proximal villages. We hope to extend future analysis to encompass the western shoreline to address the pattern of the channel's behavior (widening, etc.) within the broader context of delta system dynamics.

Geospatial Shoreline Mapping

To enhance shoreline extraction, the modified normalized difference water index (MNDWI) was

b12/16/2007 is used to estimate the early 2008 dry season shoreline because this image is the temporally closest cloud-free image.

^cTidal level data not available, but level is highly likely to be within the range of other stated levels.

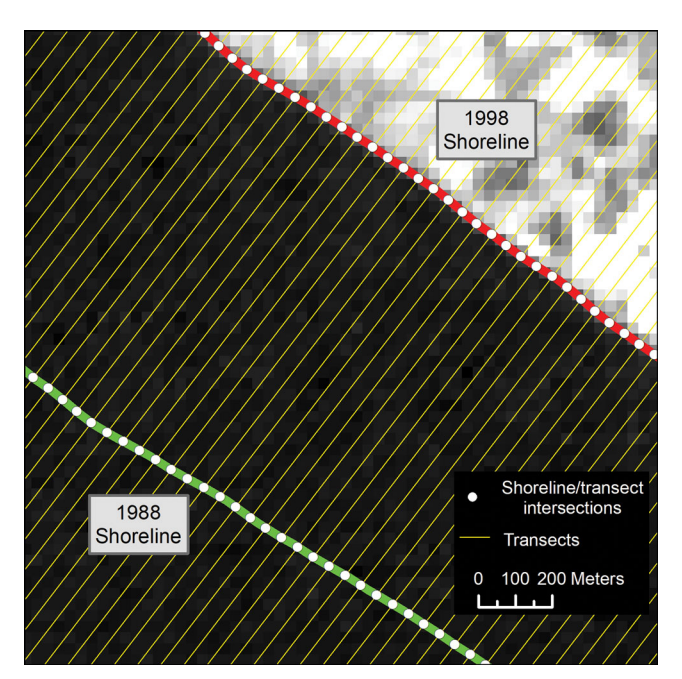


Figure 4. Example of transects at 50-m increments used for Digital Shoreline Analysis System shoreline change analysis. Landsat infrared band in background with black indicating water.

derived for each image (Xu 2006). MNDWI is commonly used to aid shoreline identification and uses the middle infrared and green bands to create an index enhancing shoreline separation. It is defined as

$$MNDWI = \frac{Green - MIR}{Green + MIR}.$$
 (1)

Six bands were used with MNDWI as input for ISODATA unsupervised classifications specified to contain ten output classes. The included bands were Blue, Green, Red, NIR, MIR, SWIR, and MNDWI. The ISODATA classification was reclassified to two classes, water and nonwater, via interactive visual inspection with the source imagery. A majority-smoothing filter was applied to clean up "salt and pepper" effects. Shorelines were derived following Daniels's (2012) shoreline extraction methodology. Gaps (i.e., breaks in the shoreline) were present at mouths of the larger tributaries. For smaller tributaries, editing was performed to extend the shorelines smoothly across gaps. Four shorelines were produced for the dry season periods of 1988, 1998, 2008, and 2018.

Quantifying Shoreline Change

Shoreline change was quantified using the Digital Shoreline Analysis System (DSAS) extension in

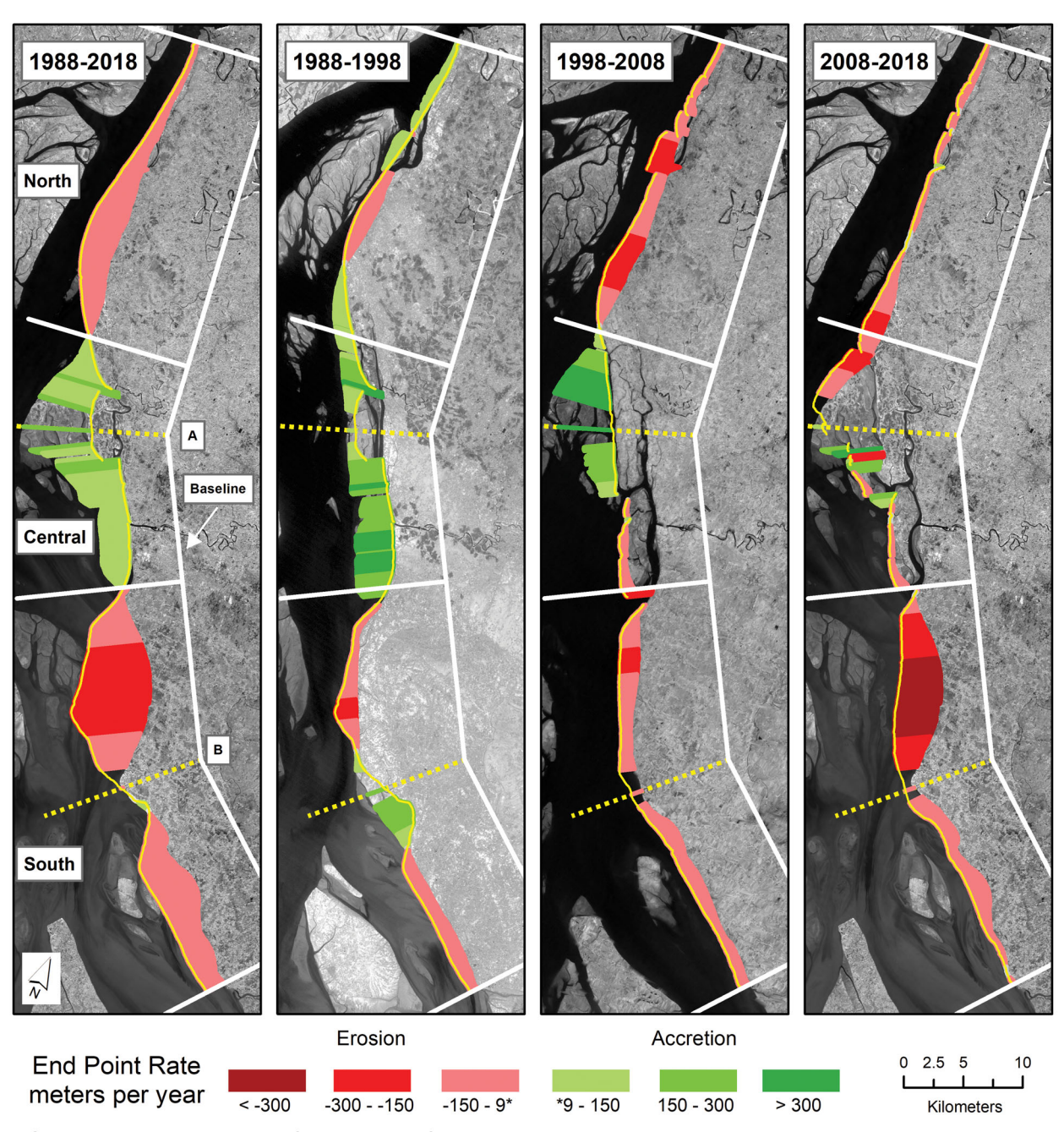
ArcGIS (Himmelstoss, Henderson, and Farris 2018). Change rates were calculated for the thirty-year period between 1988 and 2018 and decadal periods 1988 to 1998, 1998 to 2008, and 2008 to 2018. Each estimated change rate used two shoreline inputs corresponding to start and end dates. A digital baseline was created and manually located in the interior onshore area, and digital transects were cast orthogonal to the baseline at 50-m intervals for a total of 1,551 transects (Figure 4). Ideally transects extend to intersect shorelines at a 90° angle. In practice, it is rare for transect-shoreline intersections to be exactly perpendicular. We designed our linear baseline to closely parallel the shorelines by inserting inflection points (see Figure 5) so that intersections would be as close to perpendicular as possible.

Much shoreline change research, like this study, uses a 50-m interval with Landsat-derived shorelines. Other literature, primarily concerned with sand volume and associated error estimation, suggests selection of transect interval spacing based on factors such as erosion risk and human development presence. Our selection of a 50-m interval follows a large body of the prior research and accords well with the 30-m pixel resolution of Landsat imagery.

DSAS measures the distance of shoreline movement along transects enabling net shoreline movement (NSM) in meters, a measure of the distance that the shoreline has moved over time. The end point rate (EPR) used for analysis divides NSM by the intervening time between shorelines to report a shoreline change rate in meters per year. Negative values indicate erosion, and positive values indicate accretion. For a small number of transects, there were cases where zero or one shoreline was present due to gaps (i.e., unclassified or mapped shoreline). These situations are reported as gaps.

Shoreline Accuracy Assessment

Assessing shoreline accuracy for historical imagery presents challenges due to the impossibility of field-based ground truthing and the absence of very high-resolution imagery for this region prior to 2000. A fuller account of shoreline accuracy will be presented in a separate publication (but see Crawford and Rahman 2017). To summarize, a first approach assessed accuracy for a February 2000 Landsat image. Shoreline derived from a SPOT 10-m panchromatic



Solid yellow lines are shorelines for initial years of the period.

A & B: dashed lines are transects extending from inflection points of the white Baseline.

Background images are Landsat infrared bands for terminal years.

Note: The "*" in the legend for the lowest erosion/accretion classes indicates that this lower/upper bound is approximate. As described in text, a 90m net shoreline movement defined accretion/erosion events. Over 10 years, this is equivalent to EPR = plus or minus 9.0 assuming exact anniversary dates. Over the full 30 year period, this is equivalent to EPR = plus or minus 3.0.

Figure 5. Shoreline change and end point rates (m/year), 1988–2018. Note: EPR = end point rate.

image from February 2000 and with a similar tidal level was used to measure Landsat-to-SPOT shoreline distance offsets using DSAS. The mean absolute distance offset was 28.6 m with a median of

22.9 m. Based on these results, the general accuracy of Landsat shorelines for 2000 and image dates used for analysis was estimated to be approximately 25 to 30 m.

Distance zone (distance from 2017 shoreline) ^a	Number of households	% of all sampled households	Minimum distance to shoreline (m)	Maximum distance to shoreline (m)	Mean distance to shoreline (m)
1: 0 – 805 m	213	52.3	42.2	800.0	405.2
2: 805–1,610 m	131	32.2	807.9	1,603.5	1,143.1
3: >1,610 m	63	15.5	1,629.0	5,269.6	2,544.9
Total for all zones	407	100.0	42.2	5,269.6	973.9

Table 4. Sample households by distance zones from 2017 shoreline

Note: aDistance units reported in meters corresponding to zone breakpoints of 0.5, 1.0, and >1.0 miles.

An additional accuracy approach was employed to account for water level differences. A set of six Landsat images from the year 2000 dry season with varying Charchanga station water levels was used to derive vector shorelines. A linear regression estimate of the relationship between mean shoreline difference and water level difference revealed that shoreline position is shifted 7 m for every 1-m difference in water level. Although it is desirable but not possible to have identical water levels for all images used for actual analysis, our attention to selecting image dates with water levels as similar as possible is important to measuring change as accurately as possible.

Based on two complementary accuracy assessment approaches identifying a general Landsat shoreline accuracy of ~25 to 30 m coupled with the 7 m per 1-m water level difference relationship, a conservative threshold was selected to determine meaningful shoreline change. We adopted a conservative threshold of a 90-m NSM to define highly probable erosion or accretion events at the transect level; in other words, real shoreline change. Transects with NSM at or lower than -90 m were classified as erosion. Transects with NSM at or higher than 90 m were classified as accretion. Transects with NSM greater than -90 m and lower than 90 m were classified as stable (i.e., no detectable change). As noted earlier, a small number of transects were classified as gaps.

Household Survey

Households were sampled from fifteen adjacent villages in Lakshmipur district located at the far southern end of our prior 80-km shoreline reach (Figure 1). The target region had a total population of approximately 40,000 according to the most recent 2011 Bangladesh census. This region was selected based on prior pilot fieldwork including an expert workshop we held in Dhaka revealing it to have experienced significant riverbank erosion.

Additionally, visual inspection of time series imagery confirmed it to be a highly erosion-prone area.

Households were selected using a stratified random spatial sampling design to survey households located within three zones defined by distance from Landsat-derived 2017 shoreline (Table 4). A total of 420 surveys were completed within the three zones. Spatial locations of thirteen households were clearly erroneous, yielding a final sample of 407 households in the three zones: Zone 1, 0.0 to 0.5 miles (n=213); Zone 2, 0.5 to 1.0 miles (n=131); and Zone 3, 1.0 to 10.0 miles (n=63). Zones closer to the shoreline were sampled more intensively to capture a strong number of households at greater erosion risk. Our spatially explicit sample was generated by an initial set of 420 latitude-longitude points randomly generated by zone using GIS software. Large-format field maps were produced to aid field navigation and household recruitment. A team of six data enumerators supervised by two project leaders was deployed. Data enumerators used the field maps and Global Positioning System to navigate to the random point locations and approach the nearest household for recruitment into the study. If a household declined participation, enumerators approached the next nearest household. The survey instrument and all human subject activities were approved by Institutional Review Board of Virginia Polytechnic Institute and State University. To address Objective 3's focus on riverbank erosion impacts within the context of the adaptive cycle's Ω -collapse phase, we focused on analysis of the following three questions selected from the full set of ninety-five multipart questions:

Q1. Since 2008, how many times has this household had to relocate due to riverbank erosion?

Q2. For the current year of 2018, how worried are you that your home will fall into the Meghna River due to riverbank erosion?

Q3: Regardless of specific future dates or years, how strongly do you believe that your house will fall into the Meghna River at some date in the future?

We also performed geospatial analysis to estimate the number of households lost to erosion by January 2019 following the May and June 2018 household survey. This was accomplished via overlaying a Landsat-derived January 2019 shoreline with household locations.

Analytical Methods

Multiple visual, descriptive, and inferential statistical methods were used characterize spatiotemporal patterns of shoreline change. We employed simple visual interpretation combined with the more rigorous Grouping Analysis tool of ArcGIS software (Environmental Systems Research Institute 2019) to define distinct regions for the thirty-year record of change (1998-2018) that are used to organized presentation throughout. We used the 1988 to 2018 EPR as the focal variable observed at the transect level as input. The method returns an F statistic for each number of potential cluster results (two to fifteen clusters) whose maximum F statistic informs selection of an optimal number of clusters (regions) and associated cluster boundaries. After defining regions, cross-tabulations by period and region with associated chi-square tests identified the presence of statistically significant differences in percentage of transect change categories (e.g., erosion vs. accretion). To identify significant regional differences in transect EPRs for each period, the Kruskal-Wallis independent samples median test was used due to our sample's violation of assumptions of normality and equal variances.

For each region and to identify significant differences in transect EPR across time, the related samples Friedman's two-way analysis of variance by ranks test was used. This nonparametric test is appropriate for repeated measures where normality and equal variance are not present. Temporal sequence analysis was used to quantify percentage frequencies of change trajectories. All transects were coded for each decade to represent change categories (e.g., E=erosion, A=accretion). For example, a transect receiving a code of AEE experienced successive decades of accretion, erosion, and erosion. Cross-tabulation of region versus code was applied with chi-square testing and interpretation. This

method identifies space—time differences in trajectories of shoreline change. All statistical tests were implemented using SPSS software. To address our Objective 3 related to human dimensions, we report and interpret survey frequency responses and the percentage of households lost to erosion by January 2019.

Results

Regional Differences

Figure 5 depicts shoreline positions and EPR by region and period. Three regions were defined visually and by ArcGIS grouping analysis. A maximum F statistic for a four-region grouping suggested an optimal grouping of four regions; however, and as described next, we report results using three regions of north, central, and south, which had the second highest F statistic. The initial four-region grouping analysis results divided our ultimately selected south region into two regions. The clear pattern of a prominent accretionary central region landform and the fact that two southern regions identified by grouping analysis both experienced high, relatively similar erosion rates informed the decision to present results for three regions. We combined the two southern regions obtained by grouping analysis into one south region. We later refer to a subregion in the south, which conforms to the grouping analysis inferential results.

Summarizing for the three regions, results show a clear pattern for 1998 to 2018 erosion dominance for north and south with accretion dominance for the central region. Figure 6 depicts by region and period the percentages of eroding and accreting transects and mean EPR.

Moderate overall erosion was present in the north, showing temporal variation by decade. The 1988 to 1998 period had a mix of erosion and accretion, with 1998 to 2008 experiencing low and medium erosion relative to highest erosion rates in the south for the latter decade. The 2008 to 2018 period was erosion dominant but at lower magnitude than the prior decade.

The central region experienced a prominent peninsular accretion lobe. The 1988 to 1998 period witnessed accreting land that extended southward. 1998 to 2008 witnessed the emergence of a prominent accreting lobe in a northern subregion of the central

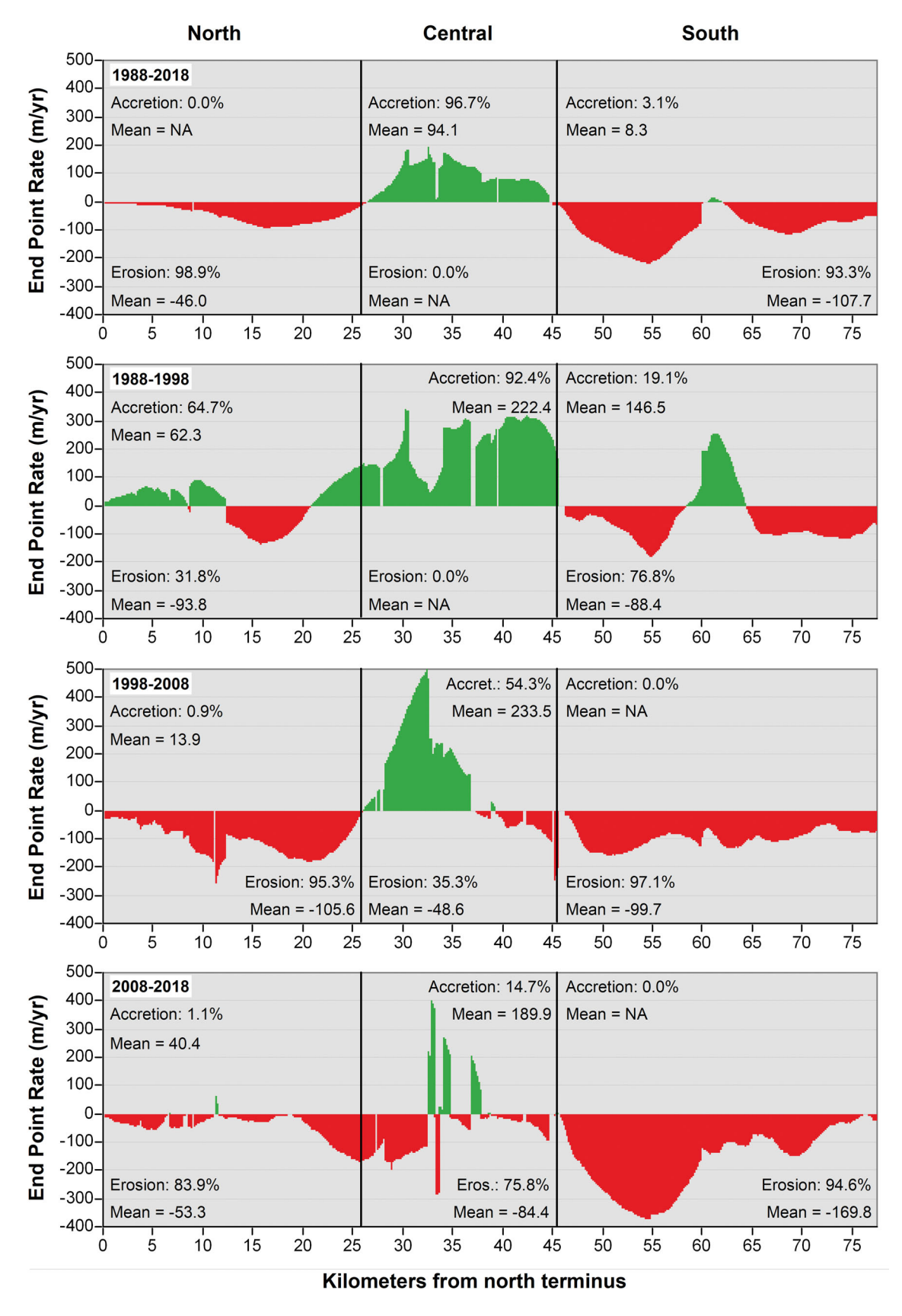


Figure 6. Shoreline change by region and period; zero kilometers on the x axis is located at the Chandpur northern terminus.

Table 5. Percentage of transects eroding or accreting, 1988 through 2018

Region/period	Erosion	Accretion	No change	Gap
1988–2018				
North $(n=529)$	98.9	0.0	0.6	0.6
Central $(n = 368)$	0.0;	96.7	0.3	3.0
South $(n=654)$	93.3	3.1	3.2	0.5
All $(N = 1,551)$	73.0	24.2	1.6	1.1
Chi-square $= 1,434$	4.7, df = 6,	p < 0.001		
1988-1998				
North $(n = 529)$	31.8	64.7	3.0	0.6
Central $(n = 368)$	0.0	92.4	0.0	7.6
South $(n = 654)$	76.8	19.1	1.8	2.3
All $(N = 1,551)$	43.3	52.0	1.8	3.0
Chi-square $= 662.1$	1, df = 6, p	< 0.001		
1998-2008				
North $(n=529)$	95.3	0.9	1.3	2.5
Central $(n=368)$	35.3	54.3	1.4	9.0
South $(n=654)$	97.1	0.0	0.0	2.9
All $(N = 1,551)$	81.8	13.2	0.8	4.2
Chi-square = 780.5	6, df = 6, p	< 0.001		
2008-2018				
North $(n=529)$	83.9	1.1	12.5	2.5
Central $(n=368)$	75.8	14.7	4.9	4.6
South $(n=654)$	94.6	0.0	4.6%	0.8
All $(N = 1,551)$	86.5	3.9	7.4%	2.3
Chi-square $= 201.2$	2, $df = 6$, p	< 0.001		

Note: Chi-square tests were run on count data (e.g., counts of transects) but are reported as percentages of total regional transect counts shown in first column to ease interpretation. Row percentages sum to 100.0% but in some cases to 100.1% due to rounding.

region coupled with southern erosion (in the central region) that had emerged in the prior decade. 2008 to 2018 experienced complex dynamics. A northern section of the emerging lobe eroded with a mix of erosion and accretion in the southern section of this lobe. Generally, the central region's lobular landform is emerging and stabilizing but migrating slightly southward. In short, this peninsular accreting subregion is a real feature.

The south experienced the highest erosion rates of any region. By decade, 1988 to 1998 was erosion dominant but with an intermediate section experiencing accretion. 1998 to 2008 saw this accretion disappear with erosion prevalent throughout. 2008 to 2018 witnessed a continued dominance of erosion with the northern subregion experiencing extreme EPR greater than 300 m per year, creating the erosional crescent evident for the full 1988 to 2018 period.

We note that our baseline contains inflection points in the central and south regions with locations that are indicated by two dashed yellow transects (Figure 5).

Shoreline Change by Region and Decade

Cross-tabulation and chi-square results revealed statistically significant differences in percentages of transect categories by region and time period the full thirty-year period (Table 5). For (1988–2018), over 90 percent of north and south transects experienced erosion compared to the central region, where 96.7 percent of transects experienced accretion. For 1988 to 1998, however, the north was accretion dominant at 64.7 percent, and the south had substantial accretion at 19.1 percent, although it was erosion dominant at 76.8 percent. The central region experienced 92.4 percent accretion during this first decade, generally consistent with the thirty-year record. For the latter two decades (1998-2008 and 2008-2018), both north and south experienced transect erosion percentages over 90 percent in most cases (the north region had 83.9 percent in 2008–2018). For these same latter two decades, central erosion increased, indicating a central pattern of initial accretion associated with the initial formation of prominent accretion, including the notable accretion of a lobular landform, followed by erosion.

Kruskal–Wallis tests revealed statistically significant differences in EPR measures by region and decade (Table 6). All multiple comparison differences were significant for the full thirty-year period (1988–2018) with the south as the most erosional region. The north's median EPR was negative, revealing it to be dominantly erosional. The central region had a positive median EPR consistent with its pattern of accretion.

For the first decade (1988–1998), all multiple comparison differences were significantly different. The north region, however, experienced positive EPR indicating accretion. The central region had a notably high median accretion rate. The south was the lone region with a negative EPR indicating erosion. For the second decade (1998–2008), the north and south both were erosional but were not significantly different from each other; both, though, were significantly different from the central region's positive EPR, indicating again central accretion. For the third decade (2008–2018), all regions had negative EPR consistent with erosion. The south, however,

Table 6.	Differences	in	EPR	by	region	and	decade	in	meters	per	vear
----------	-------------	----	------------	----	--------	-----	--------	----	--------	-----	------

	EPR 198	8–2018	EPR 1988–1998		EPR 1998-2008		EPR 2008–2018	
Region	Median ^a	M	Median ^a	М	Median ^b	М	Median ^c	М
North	-43.2	-45.7	34.1	10.6	-102.1	-103.0	-30.1	-4 5.9
Central	79.6	93.8	254.3	222.4	121.8	120.5	-33.1	-38.1
South All	−94.0 −52.1	-100.6 -36.6	-82.4 25.5	-40.8 36.6	-96.2 -84.8	−99.7 −51.2	-133.1 -59.6	-162.1 -93.8

Notes: Kruskal–Wallis independent samples median test. EPR = end point rate.

Table 7. Differences in EPR for regions across decadal time periods

Decade	All regions ^a	North ^b	Central ^b	South ^b
Time 1: 1988–1998	2.49 (36.6 m/year)	2.59 (10.6 m/year)	2.60 (222.4 m/year)	2.35 (-40.8 m/year)
Time 2: 1998–2008	1.78 (-51.2 m/year)	1.36 (–103.0 m/year)	1.93 (120.5 m/year)	2.04 (-99.7 m/year)
Time 3: 2008–2018	1.73 (-93.8 m/year)	2.05 (–45.9 m/year)	1.48 (–38.1 m/year)	1.61 (-162.1 m/year)

Notes: Related samples Friedman's two-way analysis of variance by ranks, left values are mean ranks, values in parentheses are mean EPR (m/year). EPR = end point rate.

was differentiated from the north and central regions with a significantly larger (negative) EPR.

Related samples Friedman's two-way analysis of variance by ranks tests revealed statistically significant differences in EPR over time (Table 7). This test looks at individual transect EPR values, ranks them from lowest to highest, computes mean rank by region, and tests for significant differences in regions' mean ranks. Given that negative (positive) EPR indicates erosion (accretion), lower (higher) mean ranks are generally associated with erosion (accretion). For a given transect, there are three repeated measures of EPR. The lowest EPR, which could be either negative or positive, receives rank = 1. The second lowest EPR receives rank = 2. The highest EPR receives rank = 3. Given that the three repeated measures could all be positive or all be negative, interpretation of results is facilitated by examining test results in concert with the mean EPR of each region's decadal period shown in Table 7.

For all regions combined, Time 1 (1988–1998) was significantly different from Times 2 and 3 (1998–2008 and 2008–2018), although the latter two periods did not differ significantly. Throughout we refer to mean ranks with the smallest reported numerical values as being the highest rank and largest numbers being the lowest rank; for example, a mean rank of one is the highest rank relative to a

mean rank of three, which is the lowest rank. Time 1's lowest mean rank (highest and positive mean EPR) indicates that 1988 to 1998 was a period of accretion, whereas later decades shifted to become periods of erosion.

For all regions, all multiple comparisons across periods were significantly different, although the pattern of differences varied. For the north, Time 2 had the highest mean rank (lowest and negative mean EPR) followed by Time 3 (negative mean EPR), showing that Time 2 experienced greater erosion than Time 3. Time 1's lowest mean rank (positive mean EPR) indicates it to be an initial period of accretion that was followed by periods of erosion.

For the central region, Time 1 had the lowest mean rank (highest and positive mean EPR) followed by Time 2 and then Time 3, which had the highest mean rank (lowest and negative mean EPR). Times 1 and 2 were both periods of accretion but with higher accretion rates in Time 1. Time 3 shifted to become a period of erosion.

For the south, Time 1 had the lowest mean rank (lowest and negative mean EPR) followed by Times 2 and 3. All mean EPR values were negative, indicating erosion dominance in this region. Results show that the magnitude of erosion increased significantly across the three-decadal, thirty-year period.

^aAll comparisons significantly different.

^bNorth and south not significantly different; north and south significantly different from central.

North and central not significantly different; north and central significantly different from south.

 $^{^{\}mathrm{a}}$ Times 2 and 3 not significantly different. Time 2 and Time 3 significantly different from Time 1.

^bAll comparisons significantly different.

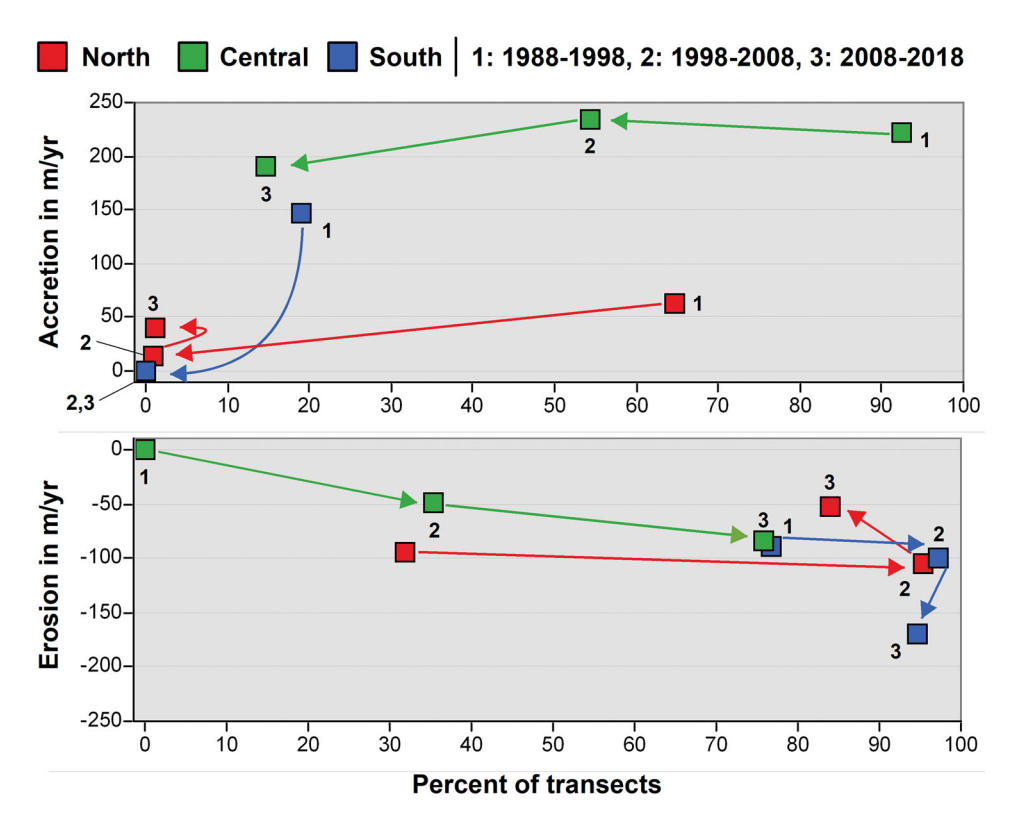


Figure 7. Temporally directed scatterplots of mean accretion and erosion end point rates.

Figure 7 depicts spatial and temporal dynamics as temporally directed scatterplots by region. This approach shows visually the same patterns as evident in the inferential statistical tests described earlier. For each region and decade, percentage of transects experiencing change (erosion or accretion) is plotted on the x axis with mean EPR plotted on the y axis. Coordinates (0, 0) indicate 0 percent of transects experiencing erosion or accretion.

Sequence Analysis of Change Trajectories

Sequence analysis enables discrimination of change trajectories by region across time (Table 8). All 1,551 transects were assigned codes describing decadal change categories where E = erosion,

A = accretion, S = stable (no detectable change), and G = gaps. For each transect, the sequential codes were concatenated, yielding a set of twenty-two code sequences empirically present in the 1,551 transects. For example, AES represents a sequence of accretion (1998–1998), erosion (1998–2008), and stable (2008–2018). The six most frequently occurring sequences represented 91.0 percent of all sequences. The remaining 9.0 percent of sequences were defined as OOO, meaning other, which are the various other sequence combinations of E, A, S, and G. This yielded seven total sequence codes in that were subjected to cross-tabulation by region and sequence. The associated chi-square test was statistically significant. For all regions combined (the total row), EEE had the highest frequency at 39.6 percent, followed

Table 8. Sequences of change trajectories by region (%)

Region	EEE	AEE	AAE	EES	AAA	AES	000	Total
North	24.8	54.1	0.9	7.0	0.0	4.7	8.5	100.0
Central	0.0	30.2	42.1	0.0	9.5	1.1	17.1	100.0
South	73.9	17.6	0.0	2.9	0.0	0.8	4.9	100.0
Total	39.6	33.0	10.3	3.6	2.3	2.2	9.0	100.0

Notes: E = erosion; A = accretion; S = stable (no detectable change); OOO = multiple other less frequent sequences. First character is 1988–1998, second character is 1998–2008, and third character is 2008–2018. Chi-square = 1,167.8, df = 12, p < 0.001.

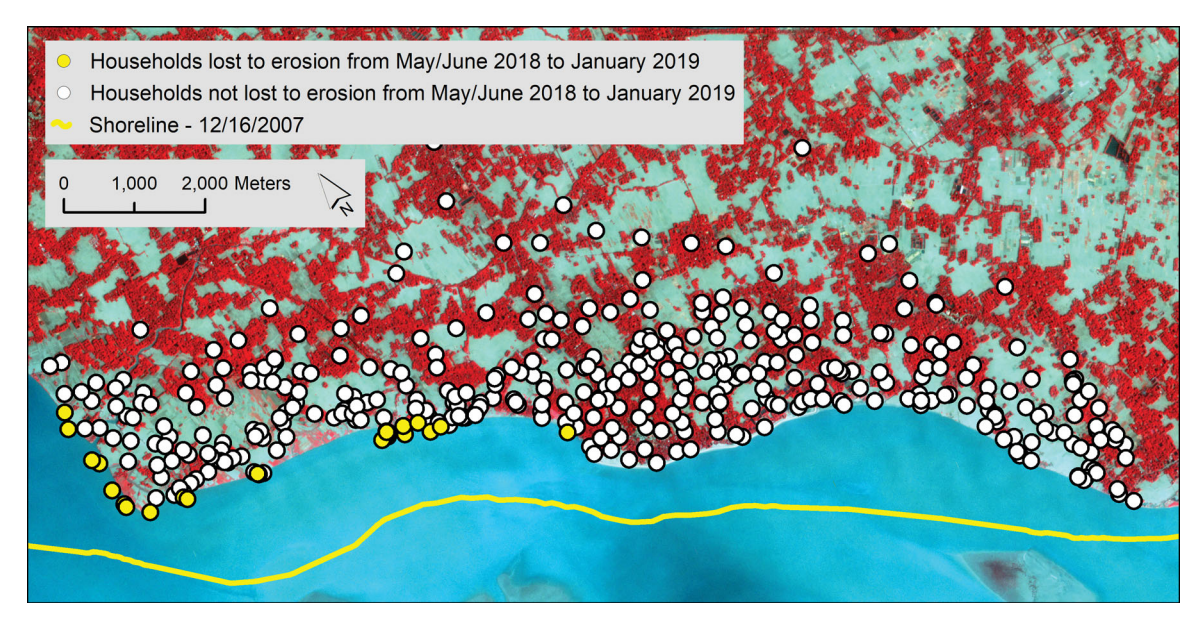


Figure 8. Households lost to erosion from May–June 2018 to January 2019: 5.9 percent of 407. Background image is a PlanetScope 3 m false color composite dated January 2019 (Planet Team 2017). Household location confidentiality was preserved by randomly shifting locations ± 50 m in the x and y directions along with the choice of map scale and point symbol size.

by AEE (33.0 percent) and AAE (10.3 percent; Table 6). These first three sequences accounted for 82.9 percent of all transects.

The south region had high frequencies of erosion dominance with EEE (73.9 percent) and AEE (17.6 percent) accounting for 91.5 percent of its transects. Excluding OOO, the central region's highest frequencies were AAE (42.1 percent), AEE (30.2 percent), and AAA (9.5 percent) accounting for 81.8 percent of its transects. The North's highest frequencies were AEE (54.1 percent) and EEE (24.8 percent) accounting for 78.9 percent of its transects. The north experienced initial accretion (1988–1998) in roughly half of its transects but thereafter was erosion dominant. The north, unlike other regions, experienced the highest frequency of stable transects, although at low percentages compared to erosion. The S for the last decade indicates shoreline stability for parts of the north that was much less present for the central or south regions.

Household Survey Results

Results reveal substantial impacts of riverbank erosion on human population. The household survey field site in the south region (Figure 8) had notably high erosion rates during 2008 to 2018. All transects spanning the extent of the household survey region were defined as eroding with a mean EPR of

 $-113.1 \,\mathrm{m/year}$ (median = -110.7, minimum = -38.2, maximum = -225.9, SD=36.3). Of the 407 total households, 43.7 percent reported at least one residential move since 2008 due to riverbank erosion (Table 9; 56.3 percent had zero moves in the bottom row). For households located in Zone 1 (closest to the shoreline), 53.1 percent experienced relocation since 2008, and 19.8 percent relocated at least two times. Results show a heightened relocation experience for households currently most proximal to the shoreline and that households more distant from the current shoreline also have prior experience of the adaptive cycle's Ω -release (collapse) phase related to riverbank erosion.

Many households experienced "worry" regarding displacement during 2018 (Table 10). The survey was conducted in May and June 2018 and asked about levels of worry regarding displacement during the remaining months of 2018 following the May and June survey. In total, 51.4 percent reported being very worried or worried. In Zone 1, 70.0 percent reported being very worried or worried, indicating a heightened perception of erosion risk for households in closer proximity to the shoreline.

A large percentage of households (85.2 percent) believed that, at some point in the future, their home would be eroded and lost to the river (Table 11). For households in Zone 1, 92.9 percent either *strongly believed* or *believed* that their home would be lost. Results for Zones 2 and 3 were lower but also high at

0.5

No. of residential moves due to riverbank erosion 0 2 3 4 Distance zone from 2017 shoreline^a 1 1: 0 - 805 m (n = 213)46.9 33.3 14.1 5.2 0.5 2: 805-1,610 m (n=131)61.8 32.1 3.8 0.8 1.5 3: >1,610 m (n=63)23.8 0.0 76.2 0.0 0.0

31.4

8.6

3.2

Table 9. Number of household residential moves since 2008 due to riverbank erosion (%)

Note: aDistance units reported in meters corresponding to zone breakpoints of 0.5, 1.0, and >1.0 miles.

56.3

All zones (n = 407)

Table 10. Percentage of households by level of worry that home will erode into the river during 2018 following the May and June 2018 survey period

	1	2	3	4	5
Distance zone from 2017 shoreline ^a	Very worried	Worried	Neutral	Not worried	Very not worried
1: 0–805 m (n = 213)	55.9	14.1	5.6	13.6	10.8
2: 805–1,610 m (n = 131)	17.5	18.3	6.9	35.1	22.1
3: >1,610 m (n=63)	9.5	11.1	1.6	49.2	28.6
All zones $(n = 407)$	36.4	15.0	5.4	26.0	17.2

Note: ^aDistance units reported in meters corresponding to zone breakpoints of 0.5, 1.0, and >1.0 miles.

Table 11. Percentage of households by level of belief that home will erode into river at some point in the future

Distance zone from 2017 shoreline ^a	1 Strongly believe	2 Believe	3 Neutral	4 Do not believe	5 Strongly do not believe
1: 0-805 m (n = 213)	59.6	33.3	6.1	0.5	0.5
2: 805–1,610 m (n = 130)	25.4	52.3	18.5	3.1	0.8
3: >1,610 m (n=63)	14.3	60.3	20.6	4.8	0.0
All zones $(n = 406)$	41.6	43.6	12.3	2.0	0.5

Note: a Distance units reported in meters corresponding to zone breakpoints of 0.5, 1.0, and >1.0 miles.

77.7 percent and 74.6 percent, respectively, in terms of belief of an ultimate loss due to erosion.

In terms of estimated household loss from May and June 2018 survey fieldwork to January 2019, a total of twenty-four households (5.9 percent) were likely lost to erosion (Figure 8) focused to the north (left in Figure 8) of this subregion, which had higher erosion rates. Additionally, and as would be expected, all of these households were located in Zone 1, which experienced an 11.3 percent loss of households.

Discussion and Conclusion

Three decades of shoreline were mapped and analyzed for an 80-km stretch of the Lower Meghna estuary. Results indicate regional variation of erosion and accretion patterns with an overall dominance of erosion. We found differences in erosion and

accretion patterns between the north, central, and south regions that varied by decade and identified using descriptive and inferential methods. Erosion rates were generally larger than rates for other regions reported Table 1, in most cases much larger. Global data of coastal erosion rates are rare, although two recent studies have deployed big data approaches using Google Earth Engine's archive of historical Landsat imagery to estimate global patterns of shoreline change (Luijendijk et al. 2018; Mentaschi et al. 2018). Luijendijk et al. (2018) focused on global sandy beaches and so is not directly comparable to our region, which is not sandy; however, we note that their highest observed hotspot rate had a mean rate of $-16.0 \,\mathrm{m/year}$ (erosion) for a site in Louisiana for the period 1984 to 2016. Mentaschi et al. (2018) used a similar approach and reported change in areal rather than linear rates, finding eroded coastal land surface of 28,000 km², which is more than twice the magnitude

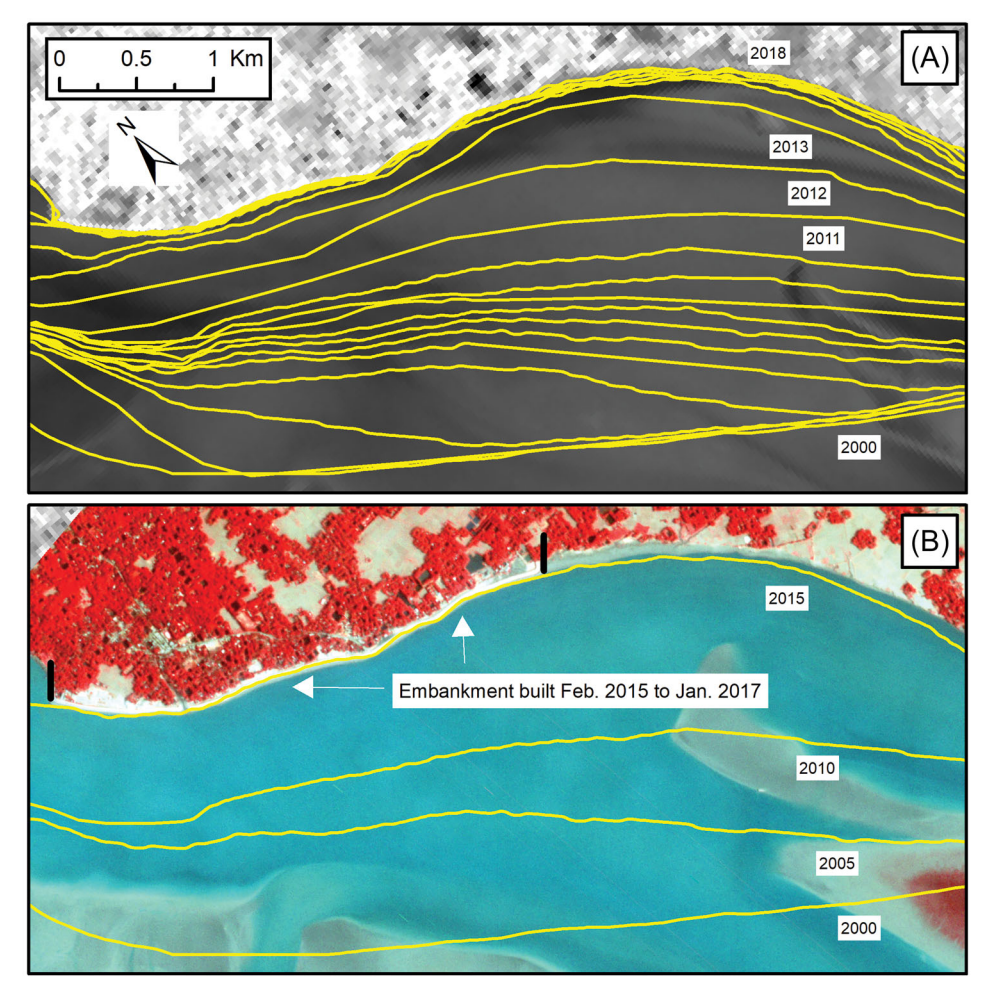


Figure 9. Shorelines at subdecadal temporal scales: (A) annual shorelines from 2000 to 2018 (selected dates not labeled for space), Landsat infrared band from January 2018 in background; (B) selected shorelines from 2000 to 2015, PlanetScope 3 m false-color image from February 2019 in background (Planet Team 2017), vertical black symbols indicate concrete embankment endpoints.

of accreting land. Our findings suggest that our nonsandy, estuarine delta study region is among the most dynamic coastlines in the world, with extreme rates of erosion in selected portions that transition households into the disruptive Ω -collapse phase of the adaptive cycle.

This work explicitly positions coastal erosion and population impacts in our study area within the theoretical framework of adaptive cycles experiencing rgrowth, K-conservation, Ω -release, and α -growth phases. In doing so, it links natural cycles to human and social cycles with an empirical focus on the Ω -release (collapse) phases related to coastal erosion and human disruption. We believe that the adaptive cycle is highly relevant to geophysical processes of delta landforms over broad time horizons and have shown that households are indeed disrupted due to erosion connected to the process of riverbank

erosion. More work is needed to empirically characterize the other cycle phases, particularly but not limited to the human dimension of how population reorganizes, regrows, and restabilizes. To do so will likely require longitudinal household data as opposed to a cross-sectional approach, although our household survey does include historical retrospective information. Although arguing merits of the adaptive cycle, we note that others who have also engaged in empirical investigation identify limits of the adaptive cycle approach (Rasmussen and Reenberg 2012; Goulden et al. 2013). For example, and in our case, is it desirable for households to repeatedly cycle through the process of erosionrelated disruption, even if it fits the pattern of the adaptive cycle (arguably not)? Imposition of a onesize-fits-all adaptive cycle can be viewed as a conservative status quo understanding that misses the



Figure 10. New embankment in Ramgati Upazila; construction started 1 February 2015 and was completed 31 January 2017.

potential for systems to leap out of the cycle or for actors to change the cycle, albeit for altered systems that still in future states might be understood by the adaptive cycle. Rasmussen and Reenberg (2012) stated for a Sahelian study that "the picture of a unidirectional process of land degradation and system collapse ... is a simplification of more complex realities" (14). Our social system in the Lower Meghna certainly involves more complexities than presented here. For example, some households (or household members) might opt out of the system by migrating to urban centers and thereby enter in to a new system. Dislocated households might also relocate in nearby and similarly vulnerable coastal sites that are eroded in short time spans such that households might not cleanly and simplistically cycle through the adaptive cycle as portrayed in Figure 2. Instead, they might be jolted in relatively short order from the α-reorganization phase directly back in to the Ω -release (collapse) phase—an unfortunate pattern of being locked (at least for some time period) into a reoccurring release–reorganization pattern. Further, power structures connected to higher social-scale political ecologies can play roles in mitigating disruptive aspects via social aid or mobilization to engineer mitigative measures such as shoreline embankment as described next.

Returning to shoreline change, our results point to the possibility of analysis at finer timescales than the decadal scale. Preliminary work has mapped shorelines annually at approximate dry season anniversary dates for 1988 to 2018 (Figure 9). Successive annual shorelines (Figure 9A) depict a continuous history of erosion; however, it is visually evident that the rate of shoreline change varies substantially by year and location. Analysis at five- or ten-year temporal resolutions misses the annual variation evident for this region. More generally, heightened attention to relevant temporal scales is important to resolve subannual, annual, and multidecadal variability (Vos et al. 2019).

The evolving CubeSat paradigm potentially provides daily imagery for much of the Earth's surface (Poghosyan and Golkar 2017). CubeSat is a moniker for a constellation of small imaging satellites. Commercial companies such as Planet Labs (Planet

Team 2017) have in recent years deployed CubeSat constellations. Figure 9B shows a PlanetScope 3 m false-color infrared image from Planet Labs taken on 3 February 2019 covering much of the extent of our household survey. A 3.5-km concrete embankment is evident as a white linear feature in the north half (left in figure) that was constructed from 1 February 2015 to 31 January 2017 (Figure 10) and effectively halted erosion for this small reach of newly embanked shoreline.

For future work, we envision transect-specific sequence code strings of length 30, one code character for each year of change in our 1988 to 2018 annual data. Transects can then be subjected to data mining methods for resulting discrete sequence data including analyses of classification and dissimilarity analysis, longitudinal entropy, and various metrics TraMiner package in available via the (Gabadinho et al. 2010; Bleisch et al. 2014; Delmelle 2016; Mas, de Vasconcelos, and Franca-Rocha 2019). Applying sequence methods to dense time series of shoreline change trajectories, or socioenvironmental change more broadly, opens rich possibilities to characterize typologies or, metaphorically, climatologies of change.

Investigation of process dynamics is beyond the scope of this study, but our team is currently investigating the role of monsoon precipitation and other process drivers. We do not view this as a limitation but rather as a reality of our stated objectives. A study limitation is the issue of shoreline positional accuracy, which we addressed in an earlier section. Although it is impossible to assess accuracy for more temporally distant shorelines, future work will produce a more robust assessment using field-based Global Positioning System data obtained for the most recent year and higher resolution imagery as available and financially feasible to obtain. Other future work points to predictive modeling of shoreline change using annual resolution shorelines with relevant predictor variables following a theory-guided data science (Karpatne et al. 2017).

In conclusion, the decadal-scale analysis presented here is an important achievement revealing statistically significant results that, beyond statistical significance, have real-world implications for vulnerable coastal populations in the Bangladesh delta. Linked (or coupled) adaptive cycles focusing empirically on the Ω -release (collapse) phase spanning human and natural systems were theoretically articulated and

demonstrated for a study area located in the largest Asian megadelta of the GBM basin. Coastal populations in Bangladesh, other densely populated Asian megadeltas, and elsewhere share similar vulnerabilities. High-quality scientific data and analysis of shoreline change can be deployed to inform mitigation and adaptation measures based on sound knowledge of historical patterns such as those presented here and projections of future change.

Acknowledgments

We thank the anonymous reviewers from the Annals of the American Association of Geographers for suggestions and Dr. Ahmed Salahuddin for his contributions during preliminary work informing this research.

Funding

This research was supported by grants from the U.S. National Science Foundation (#1660447) and the Asia-Pacific Network for Global Change Research (#ARCP2012-23NSG-CRAWFORD).

ORCID

Thomas W. Crawford http://orcid.org/0000-0002-1343-7223

References

Ackerman, J. T. 2008. Climate change, national security, and the *Quadrennial Defense Review*. Strategic Studies Quarterly 2 (1):56–96.

Ahmed, A., F. Drake, R. Nawaz, and C. Woulds. 2018. Where is the coastal? Monitoring land dynamics in Bangladesh: An integrated management approach using GIS and remote sensing techniques. Ocean & Coastal Management 151:10–24. doi: 10.1016/j.ocecoaman.2017.10.030.

Allison, M. A. 1998a. Geologic framework and environmental status of the Ganges-Brahmaputra Delta. *Journal of Coastal Research* 14 (3):826–36.

Allison, M. A. 1998b. Historical changes in the Ganges–Brahmaputra Delta front. *Journal of Coastal Research* 14 (4):1269–75.

Baki, A. B., and T. Y. Gan. 2012. Riverbank migration and island dynamics of the braided Jamuna River of the Ganges–Brahmaputra basin using multi-temporal

- Landsat images. Quaternary International 263:148–61. doi: 10.1016/j.quaint.2012.03.016.
- Bangladesh Water Development Board. n.d. Accessed September 4, 2020. https://www.bwdb.gov.bd/.
- Baral, R., S. Pradhan, R. N. Samal, and S. K. Mishra. 2018. Shoreline change analysis at Chilika Lagoon Coast, India using digital shoreline analysis system. *Journal of the Indian Society of Remote Sensing* 46 (10):1637–44. doi: 10.1007/s12524-018-0818-7.
- Bleisch, S., M. Duckham, A. Galton, P. Laube, and J. Lyon. 2014. Mining candidate causal relationships to movement patterns. *International Journal of Geographical Information Science* 28 (2):363–82. doi: 10.1080/13658816.2013.841167.
- Brammer, H. 2014. Bangladesh's dynamic coastal regions and sea-level rise. *Climate Risk Management* 1:51–62. doi: 10.1016/j.crm.2013.10.001.
- Chen, Z., and Y. Saito. 2011. The megadeltas of Asia: Interlinkage of land and sea, and human development. Earth Surface Processes and Landforms 36 (12):1703–4. doi: 10.1002/esp.2190.
- Chowdhury, M., and N. Ward. 2004. Hydro-meteorological variability in the greater Ganges–Brahmaputra-Meghna basins. *International Journal of Climatology* 24 (12):1495–1508. doi: 10.1002/joc.1076.
- Correspondent. 2019. Hundreds homeless as Meghna erosion turns serious in Laxmipur. *The Independent*, April 7. Accessed June 14, 2019. http://m.theindependentbd.com/post/194800.
- Crawford, T. W., and M. K. Rahman. 2017. Geospatial analysis of annual shoreline change in coastal Bangladesh. Paper presented at the Annual Meeting of the Association of American Geographers, Boston, April 8.
- Dada, O. A., G. Li, L. Qiao, D. Ding, Y. Ma, and J. Xu. 2016. Seasonal shoreline behaviours along the arcuate Niger Delta coast: Complex interaction between fluvial and marine processes. Continental Shelf Research 122:51–67. doi: 10.1016/j.csr.2016.03.002.
- Daniels, R. C. 2012. Using ArcMap to extract shorelines from Landsat TM data. Paper presented at the 32nd ESRI International Users Conference, San Diego, CA, July 23–27.
- Delmelle, E. C. 2016. Mapping the DNA of urban neighborhoods: Clustering longitudinal sequences of neighborhood socioeconomic change. Annals of the American Association of Geographers 106 (1):36–56. doi: 10.1080/00045608.2015.1096188.
- Environmental Systems Research Institute. 2019. How grouping analysis works. Accessed December 19, 2019. https://pro.arcgis.com/en/pro-app/tool-reference/spatial-statistics/how-grouping-analysis-works.htm.
- Esmail, M., W. E. Mahmod, and H. Fath. 2019. Assessment and prediction of shoreline change using multi-temporal satellite images and statistics: Case study of Damietta coast, Egypt. Applied Ocean Research 82:274–82. doi: 10.1016/j.apor.2018.11.009.
- Gabadinho, A., G. Ritschard, M. Studer, and N. S. Muller. 2010. Mining sequence data in R with the TraMiner package: A user's guide. University of Geneva. Accessed July 1, 2020. http://mephisto.unige.

- ch/pub/TraMineR/doc/1.8/TraMineR-1.8-Users-Guide.pdf.
- Ghoneim, E., J. Mashaly, D. Gamble, J. Halls, and M. AbuBakr. 2015. Nile Delta exhibited a spatial reversal in the rates of shoreline retreat on the Rosetta promontory comparing pre-and post-beach protection. *Geomorphology* 228:1–14. doi: 10.1016/j.geomorph. 2014.08.021.
- Goulden, M. C., W. N. Adger, E. H. Allison, and D. Conway. 2013. Limits to resilience from livelihood diversification and social capital in lake socio-ecological systems. *Annals of the Association of American Geographers* 103 (4):906–24. doi: 10.1080/00045608. 2013.765771.
- Gunderson, L. H., and C. S. Holling, eds. 2002. Panarchy: Understanding transformations in human and natural systems. Washington, DC: Island.
- Himmelstoss, E. A., R. E. Henderson, and A. S. Farris. 2018. Digital Shoreline Analysis System (DSAS) version 5.0 user guide: U.S. Geological Survey Open-File Report 2018–1179. Accessed January 10, 2020. doi: 10.3133/ofr20181179.
- Holdschlag, A., and B. M. W. Ratter. 2013. Multiscale system dynamics of humans and nature in The Bahamas: Perturbation, knowledge, panarchy and resilience. *Sustainability Science* 8 (3):407–21. doi: 10. 1007/s11625-013-0216-6.
- Holling, C. S. 1986. The resilience of terrestrial ecosystems: Local surprise and global change. In Sustainable development in the biosphere, ed. W. C. Clark and R. E. Munn, 292–317. London: Cambridge University Press.
- Hussain, M. A., Y. Tajima, K. Gunasekara, S. Rana, and R. Hasan. 2014. Recent coastline changes at the eastern part of the Meghna Estuary using PALSAR and Landsat images. IOP Conference Series: Earth and Environmental Science 20:012047. doi: 10.1088/1755-1315/20/1/012047.
- Islam, M. A., D. Mitra, A. Dewan, and S. H. Akhter. 2016. Coastal multi-hazard vulnerability assessment along the Ganges deltaic coast of Bangladesh—A geospatial approach. Ocean & Coastal Management 127:1–15. doi: 10.1016/j.ocecoaman.2016.03.012.
- Jana, A., A. Biswas, S. Maiti, and A. K. Bhattacharya. 2014. Shoreline changes in response to sea level rise along Digha Coast, Eastern India: An analytical approach of remote sensing, GIS and statistical techniques. *Journal of Coastal Conservation* 18 (3):145–55. doi: 10.1007/s11852-013-0297-5.
- Jasparro, C., and J. Taylor. 2008. Climate change and regional vulnerability to transnational security threats in Southeast Asia. Geopolitics 13 (2):232–56. doi: 10. 1080/14650040801991480.
- Jayanthi, M., S. Thirumurthy, M. Samynathan, M. Duraisamy, M. Muralidhar, J. Ashokkumar, and K. K. Vijayan. 2018. Shoreline change and potential sea level rise impacts in a climate hazardous location in southeast coast of India. *Environmental Monitoring and Assessment* 190 (1):51. doi: 10.1007/s10661-017-6426-0.
- Karpatne, A., G. Atluri, J. H. Faghmous, M. Steinbach, A. Banerjee, A. Ganguly, S. Shekhar, N. Samatova, and V. Kumar. 2017. Theory-guided data science: A

new paradigm for scientific discovery from data. *IEEE Transactions on Knowledge and Data Engineering* 29 (10):2318–31. doi: 10.1109/TKDE.2017.2720168.

- Khan, N. I., and A. Islam. 2003. Quantification of erosion patterns in the Brahmaputra–Jamuna River using geographical information system and remote sensing techniques. *Hydrological Processes* 17 (5):959–66. doi: 10.1002/hyp.1173.
- Kuehl, S. A., M. A. Allison, S. L. Goodbred, and H. Kudrass. 2005. The Ganges–Brahmaputra delta. In River deltas—Concepts models and examples, ed. L. Giosan and J. P. Bhattacharya, 413–34. SEPM Special Publication No. 83. https://doi.org/10.2110/pec.05.83
- Luijendijk, A., G. Hagenaars, R. Ranasinghe, F. Baart, G. Donchyts, and S. Aarninkhof. 2018. The state of the world's beaches. *Scientific Reports* 8 (1):6641. doi: 10.1038/s41598-018-24630-6.
- Mas, J. F., R. de Vasconcelos, and W. Franca-Rocha. 2019. Analysis of high temporal resolution land use/land cover trajectories. *Land* 8 (2):30. doi: 10.3390/land8020030.
- McGranahan, G., D. Balk, and B. Anderson. 2007. The rising tide: Assessing the risks of climate change and human settlements in low elevation coastal zones. *Environment and Urbanization* 19 (1):17–37. doi: 10. 1177/0956247807076960.
- Mentaschi, L., M. I. Vousdoukas, J. Pekel, E. Voukouvalas, and L. Feyen. 2018. Global long-term observations of coastal erosion and accretion. *Scientific Reports* 8 (1):12876. doi: 10.1038/s41598-018-30904-w.
- Mikhailov, V. N., and M. A. Dotsenko. 2007. Processes of delta formation in the mouth area of the Ganges and Brahmaputra rivers. *Water Resources* 34 (4):385–400. doi: 10.1134/S0097807807040033.
- Natesan, U., A. Parthasarathy, R. Vishnunath, G. E. J. Kumar, and V. A. Ferrer. 2015. Monitoring longterm shoreline changes along Tamil Nadu, India using geospatial techniques. *Aquatic Procedia* 4:325–32. doi: 10. 1016/j.aqpro.2015.02.044.
- Paul, B. K., and H. Rashid. 2017. Climatic hazards in coastal Bangladesh: Non-structural and structural solutions. Oxford, UK: Elsevier.
- Permanent Service for Mean Sea Level. n.d. Accessed August 20, 2018. https://www.pmsl.org/.
- Planet Team. 2017. Planet application program interface: In space for life on Earth. San Francisco, CA: Planet. Accessed July 1, 2019. https://api.planet.com.
- Poghosyan, A., and A. Golkar. 2017. CubeSat evolution: Analyzing CubeSat capabilities for conducting science missions. *Progress in Aerospace Sciences* 88:59–83. doi: 10.1016/j.paerosci.2016.11.002.
- Qiao, G., H. Mi, W. Wang, X. Tong, Z. Li, T. Li, L. Shijie, and Y. Hong. 2018. 55-Year (1960–2015) spatiotemporal shoreline change analysis using historical DISP and Landsat time series data in Shanghai. *International Journal of Applied Earth Observation and Geoinformation* 68:238–51. doi: 10.1016/j.jag.2018.02.009.
- Rahman, A. F., D. Dragoni, and B. El-Masri. 2011. Response of the Sundarbans coastline to sea level rise

- and decreased sediment flow: A remote sensing assessment. Remote Sensing of Environment 115 (12):3121–28. doi: 10.1016/j.rse.2011.06.019.
- Rani, M., S. Rehman, H. Sajjad, B. S. Chaudhary, J. Sharma, S. Bhardwaj, and P. Kumar. 2018. Assessing coastal landscape vulnerability using geospatial techniques along Vizianagaram–Srikakulam coast of Andhra Pradesh. *Natural Hazards* 94 (2):711–25. doi: 10.1007/s11069-018-3414-9.
- Rasmussen, L., and A. Reenberg. 2012. Collapse and recovery in Sahelian agro-pastoral systems: Rethinking trajectories of change. *Ecology and Society* 17 (1):14. doi: 10.5751/ES-04614-170114.
- Salauddin, M., K. T. Hossain, I. A. Tanim, M. A. Kabir, and M. H. Saddam. 2018. Modeling spatio-temporal shoreline shifting of a coastal island in Bangladesh using geospatial techniques and DSAS extension. Annals of Valahia University of Targoviste, Geographical Series 18 (1):1–13. doi: 10.2478/avutgs-2018-0001.
- Sarker, H. Q., I. Huque, M. Alam, and R. Koudstaal. 2003. River, chars, and char dwellers of Bangladesh. *International Journal of River Basin Management* 1 (1):61–80. doi: 10.1080/15715124.2003.9635193.
- Sarwar, M., and C. D. Woodroffe. 2013. Rates of shore-line change along the coast of Bangladesh. *Journal of Coastal Conservation* 17 (3):515–26. doi: 10.1007/s11852-013-0251-6.
- Small, C., D. Sousa, G. Yetman, C. Elvidge, and K. MacManus. 2018. Decades of urban growth and development on the Asian megadeltas. Global and Planetary Change 165:62–89. doi: 10.1016/j.gloplacha. 2018.03.005.
- Smith, P. J. 2007. Climate change, weak states and the "War on Terrorism" in South and Southeast Asia. Contemporary Southeast Asia 29 (2):264–85. doi: 10. 1355/CS29-2C.
- Stevens, F. R., A. E. Gaughan, C. Linard, and A. J. Tatem. 2015. Disaggregating census data for population mapping using random forests with remotely-sensed and ancillary data. *PLoS ONE* 10 (2):e0107042. https://doi.org/10.1371/journal.pone. 0107042.
- Sundstrom, S., and C. R. Allen. 2019. The adaptive cycle: More than a metaphor. *Ecological Complexity* 39:100767. doi: 10.1016/j.ecocom.2019.100767.
- Ullah, M. W., M. S. Islam, and M. A. Alam. 2019. Recent developments in GIS capabilities in water sector in Bangladesh—CEGIS the pioneer. Paper presented at the 2nd International Conference on Water and Environmental Engineering, Dhaka, Bangladesh, January 19–22.
- U.S. Geological Survey (USGS). 2018. USGS Global Visualization Viewer. Accessed August 20, 2018. https://glovis.usgs.gov/.
- Vos, K., M. D. Harley, K. D. Splinter, J. A. Simmons, and I. L. Turner. 2019. Sub-annual to multi-decadal shoreline variability from publically available satellite imagery. *Coastal Engineering* 150:160–74. doi: 10. 1016/j.coastaleng.2019.04.004.

Wilde, K. D. 2000. Out of the periphery: Development of coastal chars in southeastern Bangladesh. Dhaka, Bangladesh: University Press Limited.

Wilde, K. D. 2011. Moving coastlines: Emergence and use of land in the Ganges-Brahmaputra Meghna estuary. Dhaka, Bangladesh: University Press Limited.

Wilson, C. A., and S. J. Goodbred, Jr. 2015. Construction and maintenance of the Ganges–Brahmaputra–Meghna delta: Linking process, morphology, and stratigraphy. *Annual Review of Marine Science* 7:67–88. doi: 10.1146/annurev-marine-010213-135032.

Woodroffe, C. D. 2010. Assessing the vulnerability of Asian megadeltas to climate change using GIS. In Coastal and marine geospatial technologies, ed. D. R. Green, 379–91. New York: Springer.

Woodroffe, C. D., R. J. Nicholls, Y. Saito, Z. Chen, and S. Goodbred. 2006. Landscape variability and the response of Asian megadeltas to environmental change. In *Global change and integrated coastal management*, ed. N. Harvey, 277–314. New York: Springer.

ment, ed. N. Harvey, 277–314. New York: Springer. Woodroffe, C. D., and Y. Saito. 2011. River-dominated coasts. Treatise on Estuarine and Coastal Science 3:117–35.

Xu, H. 2006. Modification of normalised difference water index (NDWI) to enhance open water features in remotely sensed imagery. *International Journal of Remote Sensing* 27 (14):3025–33. doi: 10.1080/01431160600589179.

Zhang, X., Z. Yang, Y. Zhang, Y. Ji, H. Wang, K. Lv, and Z. Lu. 2018. Spatial and temporal shoreline changes of the southern Yellow River (Huanghe) Delta in 1976–2016. *Marine Geology* 395:188–97. doi: 10.1016/j.margeo.2017.10.006.

THOMAS W. CRAWFORD is a Professor in the Department of Geography at Virginia Polytechnic Institute and State University, Blacksburg, VA 24061. E-mail: tomc3@vt.edu. His research interests include coastal hazards, vulnerability, and resilience and geospatial applications.

MUNSHI KHALEDUR RAHMAN is an Assistant Professor in the Department of Geology and Geography at Georgia Southern University, Statesboro, GA 30458. E-mail: mkrahman@georgiasouthern.edu. His research interests include the study of nature—society interactions, vulnerability and resilience, application of geospatial technologies, and spatial analysis.

MD. GIASHUDDIN MIAH is a Professor in the Department of Agroforestry and Environment and the Vice Chancellor currently is of Bangabandhu Sheikh Mujibur Rahman Agricultural Gazipur-1706, Bangladesh. University, giash1960@gmail.com. His research interests include climate change, land use, ecosystem management, resource use in agroforestry, livelihoods, food security.

MD. RAFIQUL ISLAM is a Professor in the Department of Agronomy at Bangabandhu Sheikh Mujibur Rahman Agricultural University, Gazipur-1706, Bangladesh. E-mail: rafiarib@yahoo.com. His research interests include natural resource management, geospatial analysis and climate-smart agriculture, agro-ecosystem management, and livelihood development of the rural community.

BIMAL KANTI PAUL is a Professor in the Department of Geography and Geospatial Sciences at Kansas State University, Manhattan, KS 66506. E-mail: bkp@ksu.edu. His research interests include human—environment interactions, population and health geographies, and global climate change.

SCOTT CURTIS is a Distinguished Professor of Natural Sciences and Mathematics the Department of Geography, Planning, and Environment East Carolina University, at Greenville, NC 27858. E-mail: curtisw@ecu.edu. His research seeks to understand how water hazards and hydroclimatic variability and change affect society.

MD. SARIFUL ISLAM is a PhD Candidate in the Geospatial and Environmental Analysis Program in the Department of Geography at Virginia Tech, Blacksburg, VA 24061. E-mail: shariful@vt.edu. His research interests include coastal hazards, remote sensing and GIS, and human–environment interactions.